Computers & Graphics (2024)

Contents lists available at ScienceDirect

Computers & Graphics

journal homepage: www.elsevier.com/locate/cag

# Interior control structure for Generalized Bézier patches over curved domains

Márton Vaitkus*, Péter Salvi, Tamás Várady

*Budapest University of Technology and Economics*

ARTICLE INFO

*Article history*:
Received May 14, 2024

*Keywords:* Multi-sided Surfaces, Curved Domain, Medial Axis Transform, Template, Interior Control

ABSTRACT

Generalized Bézier patches with curved domains can represent complex, multi-sided surfaces, but do not provide explicit control over the interior of the surface, as they are defined by means of side-based ribbons. In this paper we extend this representation by proposing a uniform, intuitive control structure, based on *templates* – a collection of quadrilaterals that covers and affects the 3D shape. It is constructed based on a variant of the Medial Axis Transform (MAT) that uses the local parameterization of the domain. For a given patch a hierarchical sequence of 2D templates can be defined, each determining the topology of the corresponding 3D control structure. First we introduce templates, then present the way of associating biparametric Bernstein blend functions with the control points. Next we describe how to position the control points of the MAT skeleton and the remaining interior control points, while ribbons are preserved. Finally we show a few examples that demonstrate the method and discuss the pros and cons of the approach.



## 1. Introduction

A significant part of free-form shapes in Computer Aided Geometric Design is represented by control point based surfaces, such as Bézier or B-spline patches, defined by quadrilateral grids of control points. These surfaces are not always suitable to represent shapes with general topology, and this has motivated the development of multi-sided surfacing schemes supporting more complex control structures. We refer to a recent survey paper by the current authors [1], where the state of the art in genuine multi-sided modeling is presented.

The majority of multi-sided patches is defined over a convex polygonal domain, and the control points are generally arranged into a rotationally symmetric *spiderweb* structure of quadrilaterals, see for example Zheng and Ball [2], Várady et al. [3]. In the last few years it has been recognized that convex domains may have shape limitations for certain shape configurations; this led to the Generalized Bézier and B-spline patches over curved domains [4, 5]. Here the input is a set of *ribbon surfaces* that prescribe positional and cross-derivative constraints along the boundaries, and their combination yields the multi-sided patch. Ribbons are generally given as a grid of control points in order to match adjacent patches; for the interior, however, no control points are available – in other words, curved domain patches are fully determined by the ribbons. This may be an advantage, as no further effort is needed to finalize the patch, but it can be a disadvantage, when the patch interior is not satisfactory.

In this paper we propose an intuitive control structure for Curved Domain Generalized Bézier patches [4] (abbreviated as CD-GB) that is – in some sense – analogous to spiderwebs, and contains interior control points placed over the 'underdefined' parts of the patch. This structure corresponds to the layout of the shape and thus supports intuitive editing. The representation can be refined, then it can be used for various high-level operations, such as approximation of point clouds or trimmed surfaces, manual design and interior fairing.

*Corresponding author:
*e-mail:* vaitkus@iit.bme.hu (Márton Vaitkus)

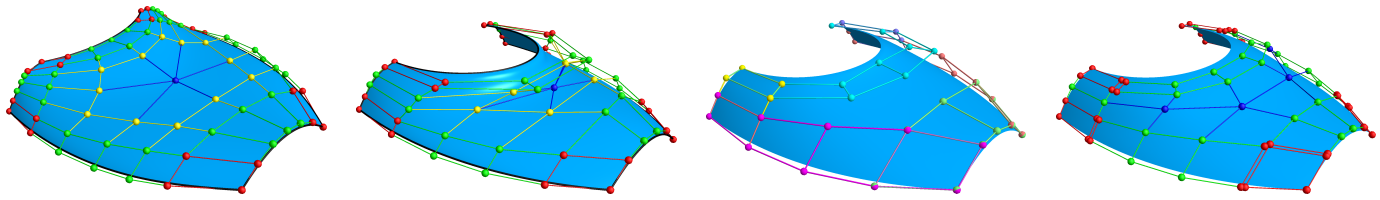

(a) Patch over a convex domain spiderweb, fair surface

(b) Patch with a large concave arc, convex domain, spiderweb yields awkward control structure, poor surface

(c) Same patch as (b), curved domain, ribbons only, fair surface

(d) Same patch as (b), curved domain, MAT-based control structure, fair surface

Figure 1: Control structures for Generalized Bézier patches.

Our concept is visualized in Figure 1 (control point coloring will be explained later). Fig. 1a shows a Generalized Bézier patch with a convex domain and a full spiderweb control structure; it has a single central control point in the middle. Fig. 1b shows a variant of the patch with a strong concave arc; here the use of a convex domain and a single middle control point is not sufficient as indicated by the backfolding surface and the awkward control structure. Fig. 1c shows a variant of the previous patch using the CD-GB representation [4], combining six input ribbons into a much nicer shape. In Fig. 1d, finally our proposed curved domain GB patch is presented that uses an interconnected control structure, with four interior control points distributed in a natural manner.

The main contributions of the paper are the following. We introduce a *parametric MAT* structure that is built on the parameterization of a curved domain. By means of this MAT, we derive a topological structure of quadrilaterals over the domain, and generate a sequence of 2D *templates*. Each template corresponds to a 3D structure of control points that can incorporate boundary ribbons, while also providing an additional set of interior control points. Templates constrain the longitudinal degrees of the boundaries, thus input ribbons may need to be elevated or reduced to meet these constraints. For each interior control point we assign a blend function composed of Bernstein polynomials, and use these to redistribute the weight deficiency generated by the ribbon blending functions. We propose methods to position the interior control points in 3D, and investigate the editing and refinement of the template structures.

The paper is structured as follows. After reviewing related work (Section 2), we revisit the equation for CD-GB patches and show how it needs to be modified (Section 3). In Section 4 we discuss parametric MAT structures and template topologies. In Sections 5 and 6 we present the blending functions and the placement of the interior control points, respectively. We show a few examples and discuss special cases in Section 7. Some interesting open issues conclude the paper.

## 2. Related work

In this section we focus exclusively on multi-sided surfaces that are defined by control points. For a detailed survey of various representations see [1]. Basically, there are three groups of approaches – *side-based* schemes arrange control point structures along their boundaries (see e.g. Fig. 1c), *corner-based* schemes place control points around the corners, while in *interconnected* patches the control points cover and influence the shape over the entire domain (see e.g. Fig. 1a or 1d).

Interconnected patches are generally defined over convex polygonal domains. There exist a variety of interconnected topological structures [6], including Minkowski sums [7], lattice polygons [8], triangular spiderwebs [9] and rectangular spider-webs [10, 2, 3, 11, 12]. Rectangular spiderwebs offer a particularly natural generalization of standard tensor-product surfaces, which can easily incorporate Bézier ribbon constraints. Interconnected constructions are generally limited to regular or convex polygonal domains and centrally symmetric control structures. Our approach is inspired by the Generalized Bézier (GB) patches introduced by Várady et al. [3] using a rectangular spiderweb control structure over regular polygonal domains. Follow-up works have generalized GB patches to concave polygons (CGB patches) [13] and even curved domains (CD-GB patches) [4]. The CD-GB scheme is fundamentally side-based (see Section 3 for details) and thus lacks a natural method for controlling the patch interior – our goal is to add an interconnected control structure that is appropriate for curved domains, as well.

There exist a variety of approaches for constructing blending functions within a general domain interior, related to 'mesh-free' approximation of scattered data [14], as well as (bi)harmonic transfinite interpolation [15, 16]. However, we are not aware of any work that integrated these kinds of interior degrees of freedom into a coherent generalized Bézier control structure.

For multi-sided patches the blending functions often do not form a partition of unity – this is generally handled via normalization [8, 9, 17] or by assigning the weight deficiency to a single control point [18, 3]. Zheng and Ball [2] have proposed to distribute the weight deficiency of their particular construction between interior vertices in a rectangular spiderweb control structure, and later also derived degree elevation rules based on this approach [19]. Similar ideas have been applied to convex GB patches as well [17]. Salvi [20] introduced a 'hybrid' patch, where a subset of the blending functions of a convex GB patch [3] is used for transfinite interpolation and the remaining control points distribute the weight deficiency over the interior. It is also possible to use the weight deficiency (or any function that vanishes along the domain boundary) to blend an interior surface while retaining boundary interpolation, which is a common practice in geometric modeling [21, 22], as well as

in numerical analysis [23]. Our approach distributes the weight deficiency among elements of a control structure naturally associated with a curved parametric domain.

The original Generalized Bézier construction [3] included a simple degree elevation rule that provided an initial setting for the interior control points based on input ribbons, and also allowed for hierarchical editing. We will present a method for the refinement of curved domain patches that operates in an analogous fashion.

An important part of our method is a decomposition of the domain into quadrilateral regions, which is an active area of research – see Campen [24]. We aim to create a simple, easily refinable quadrangulation that is compatible with Bézier boundaries of different degrees. State-of-the-art optimization-based quadrangulation methods [25, 26] can produce high-quality layouts suitable for e.g. subdivision surfaces [27], but typically have a topological structure that makes it challenging to associate bi-parametric blend functions with the vertices. Quadrilateral decompositions of planar domains were also studied in relation to multi-patch parameterizations for isogeometric analysis, see e.g. Buchegger and Jüttler [28] where a layout topology is selected based on the parametric distortion of an optimized template mapping.

Another family of methods finds solutions with a fixed number of quads along each side via an integer programming problem, as surveyed in the recent work of Tarini [29] – however, such approaches appear to be limited to (domains subdivided into) convex polygons. A wide range of quadrangulation methods are based on the Medial Axis Transform (MAT) of the domain, e.g. [30, 31, 32, 33]. Our own approach for template generation shows many similarities with such MAT-based techniques; an important difference is that instead of the usual Euclidean MAT, we use a medial axis based on local distance parameters that we believe to be novel.

## 3. Revisiting and extending CD-GB patches

A CD-GB patch [4] is a multi-sided surface that interpolates boundary curves and cross-derivative functions along them. The boundaries and the associated constraints are given in the form of Bézier *ribbons*: quadrilateral Bézier patches of (independently) arbitrary degrees, one for each boundary ($i = 1 \dots n$):

$$\mathbf{R}_i(s,h) = \sum_{j=0}^{d_i} \sum_{k=0}^{e_i} \mathbf{C}^i_{j,k} \cdot B^{d_i}_j(s) B^{e_i}_k(h). \tag{1}$$

Here $d_i$ and $e_i$ are the degrees along the boundary and in the cross-direction, respectively; $\mathbf{C}^i_{j,k}$ is the $j$-th control point in the $k$-th row, and $B^d_j(t)$ is the $j$-th Bernstein polynomial of degree $d$. Note that except for the corner positions, the ribbons do not have to be compatible.

The patch itself is the normalized sum of $n$ *interpolant* surfaces. The equation for these is very similar to that of the ribbons, but the cross-directional degree is $d^\perp_i > 2e_i$, and a weighting function ($\mu^i_j$) is employed to cancel the interpolant's contribution to the adjacent boundaries (see details below):

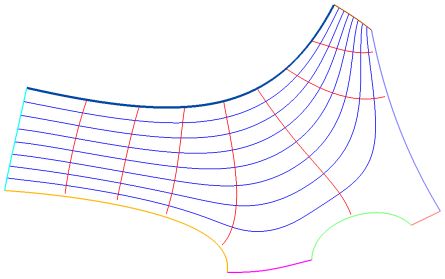

Figure 2: Local parameterization relative to the top side: $s$- and $h$-parameter isolines are shown in red and blue, respectively. The surface generated by this domain will be shown later in Section 7.

$$\begin{aligned}\mathbf{I}_i(s_i,h_i) &= \sum_{j=0}^{d_i} \sum_{k=0}^{e_i} \mathbf{C}^i_{j,k} \cdot \underbrace{\mu^i_j(u,v) B^{d_i}_j(s_i) B^{d^\perp_i}_k(h_i)}_{\text{denoted by } \gamma_{ijk}(u,v)} \\ &=: \sum_{j=0}^{d_i} \sum_{k=0}^{e_i} \mathbf{C}^i_{j,k} \gamma_{ijk}(u,v). \end{aligned} \tag{2}$$

Adding these together requires a mapping to/from a common domain. The CD-GB patch uses a domain that is bounded by curves in the $(u,v)$ plane and mimics the 3D boundary configuration. The local parameter mappings $s_i = s_i(u,v)$ and $h_i = h_i(u,v)$ are called the *side* and *distance parameters*. The former varies linearly between 0 and 1 along the associated *base side* of the domain, while the latter vanishes on that side and increases as we move inside the domain, reaching 1 at the 'far sides', i.e., sides not adjacent to the base side (all except $i-1$, $i$ and $i+1$), see Fig. 2.

For details on domain generation and parameterization, see the original paper [4]. As for the weights, a simple option is to use rational functions (similar to Gregory twists [34])

$$\mu^i_j(u,v) = \begin{cases} h^\ell_{i-1} / \left(h^\ell_{i-1} + h^\ell_i\right) & \text{when } j < \ell, \\ h^\ell_{i+1} / \left(h^\ell_{i+1} + h^\ell_i\right) & \text{when } j > d_i - \ell, \\ 1 & \text{otherwise,} \end{cases} \tag{3}$$

where $\ell$ is the order of interpolation: this term cancels the contribution of up to $\ell-1$ derivatives on the adjacent sides, ensuring that the resulting patch only depends on ribbon $i$ when evaluated at a domain point on side $i$. Alternative schemes with similar properties are described in Várady et al. [4].

The patch itself is then written as

$$\mathbf{S}(u,v) = \frac{1}{\Gamma(u,v)} \cdot \sum_{i=1}^{n} \mathbf{I}_i(s_i,h_i), \tag{4}$$

where

$$\Gamma(u,v) = \sum_{i=1}^{n} \sum_{j=0}^{d_i} \sum_{k=0}^{e_i} \gamma_{ijk}(u,v). \tag{5}$$

Normalization is needed to ensure the affine invariance property, as generally $\Gamma(u,v) \neq 1$ in the interior of the domain. In our work we use the *weight deficiency* $(1 - \Gamma(u,v))$ to add interior controls to the surface, as follows.

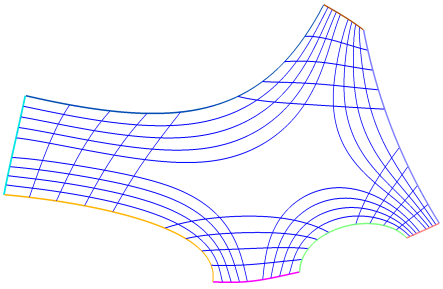

(a) $h_i$ isolines (in the range $[0.1, 0.4]$)

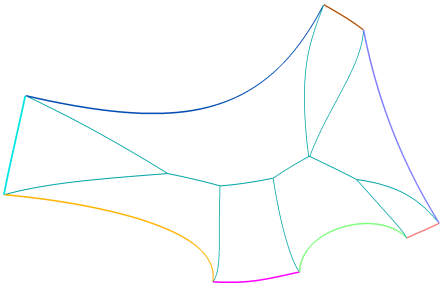

(b) Parametric medial axis (MA)

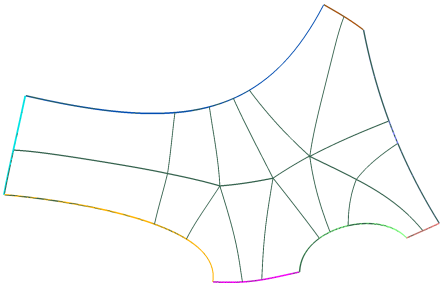

(c) Tiling by $s_i$-lines dropped from MAT vertices

Figure 3: Steps of the quadrangulation.

Assuming that we have *interior control points* $\mathbf{C}_l^{\text{Int}}$, $l = 1 \dots L$, and associated *interior blending functions* $\omega_l(u, v)$, we can modify Eq. (4):

$$\mathbf{S}(u, v) = \sum_{i=1}^{n} \mathbf{I}_i(s_i, h_i) + (1 - \Gamma(u, v)) \cdot \frac{1}{\Omega(u, v)} \sum_{l=1}^{L} \mathbf{C}_l^{\text{Int}} \omega_l(u, v), \qquad (6)$$

where dividing by $\Omega(u, v) = \sum_{l=1}^{L} \omega_l(u, v)$ normalizes the interior blending functions to sum to unity. In other words, we distribute the weight deficiency of the original patch $(1 - \Gamma(u, v))$ between the interior control points $\mathbf{C}_l^{\text{Int}}$, and the relative magnitudes of the $\omega_l$ blends define the proportion of their individual share.

In the following sections we will discuss how the interior control points are defined and what sort of blending functions are assigned to them.

## 4. MAT-based template structures

In this section we describe how the topological structure of the control net is created. We assume that the input ribbons are given and a curved domain has already been computed, together with a parameterization $(s_i, h_i)$ for each side of the domain. Details of these steps can be found in the CD-GB paper [4].

### 4.1. Template hierarchy

We generate a type of MAT (Medial Axis Transform) graph in the domain, with the crucial difference compared to the traditional MAT [35] that instead of the Euclidean distance measure, we consider *parametric* distances given by the $h_i$ coordinates. (Note that we use the term 'MAT' for the medial axis even without the associated distances, following common practice.) The *parametric MAT* is a tessellation of the domain similar to a Voronoi diagram, where each *edge* represents the locus of points that are at an *equal distance* (in parametric sense) from two boundaries, and each *vertex* represents points where the parametric distances from three or more boundaries are equal (i.e., where three or more edges intersect). The interior vertices of the parametric MAT graph are referred to as the *skeleton*. Figure 3a shows the $h_i$ isolines, and Figure 3b shows the medial axis structure.

The parametric MAT suggests a natural quadrilateral decomposition of the domain by connecting the skeleton vertices with boundary *footpoints* – a straightforward way to do so is to trace isolines of the $s_i$ coordinates from a given vertex, but note that the geometry of the domain decomposition is not relevant for what follows. Quadrilateral cells will be created at the corners, along with pairs of quadrilaterals that topologically connect two segments of opposing boundaries, sharing a skeleton edge, see our example in Figure 3c. This topological structure is also called the *T2 template*, consisting of a perimeter loop of boundary curves and the skeleton in the middle. In general, *TD* denotes a structure of *depth D*, indicating how many layers of vertices are produced. As it will be explained shortly, the depth equals the cross-directional degree of the blending functions.

The *T2* topology (see Figure 4a) can be refined using a *topological* subdivision rule inspired by Bézier degree elevation: new vertices are created for each quadrilateral cell, as well as each boundary edge, and the newly introduced vertices – together with the corner vertices – are connected based on the topological dual of the previous structure. This subdivision is for now purely topological – explicit subdivision rules applied to corresponding *control points* will be introduced in Section 6.1.

The first subdivision yields the *T3* structure ($D = 3$), having two layers of edges, with a sequence of polygons appearing in the place of the skeleton. For each polygonal face of *T3* the number of sides is equal to the valence of the corresponding skeleton vertex, see our example in Figure 4b. We can iterate the refinement process, yielding *T4* ($D = 4$), which has two layers of vertices, with skeleton points reappearing as the centroids of the *T3* polygons (Figure 4c). In Figure 4d we also show the *T5* structure.

This refinement procedure defines a sequence of templates of depth $D$ with $\lfloor D/2 \rfloor$ layers, i.e., there are $\lfloor D/2 \rfloor$ quads on both sides of the medial structure, which itself is represented by a polyline connecting the skeleton vertices, when $D$ is even, and with a sequence of multi-sided polygons (the duals of the skeleton vertices), when $D$ is odd.

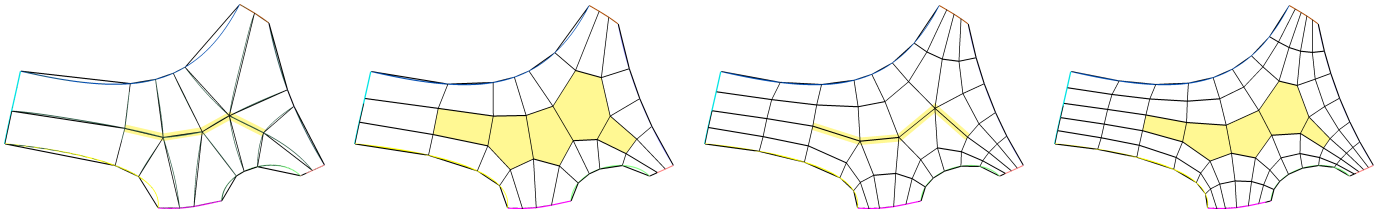

(a) *T2* (b) *T3* (c) *T4* (d) *T5*

Figure 4: Illustration of the topology in a template sequence with the medial structure in yellow.

We would like to emphasize that this sequence of templates can be constructed directly from a curved domain and its local parameterization, and furthermore that only the *topology* of the domain templates will be relevant for our purposes.

### 4.2. Relating templates to CD-GB patches

In this section we explain how the correspondence between a template topology and a Generalized Bézier control structure is established. Let us assume that the template vertices represent the control points of some multi-sided surface capable of reproducing Bézier boundaries (the blending functions will be specified later). If a side of the template boundary contains three vertices, the template can represent a quadratic Bézier curve along that side; if there are four vertices (i.e., two footpoints and two corners) the template boundary can represent a cubic curve and so on. In general the representable degree is equal to the number of footpoints plus one.

This means that the quadrangulation of the template imposes constraints on the degrees of the 3D boundaries. For example in Figure 4a, *T2* can represent a patch with degrees 2,3,3,4,2,3,2,5 (counting counter-clockwise, starting from the cyan edge). *T3* has degrees 3,4,4,5,3,4,3,6 and so on, see Figure 4b. We call these the *target degrees* ($d^{TD}$) of depth $D$, or just $d^T$ when the depth is not specified.

The input ribbons have pre-defined *input degrees* ($d^I$) in their longitudinal direction. In order to incorporate the ribbons into a template structure with a given depth, the input and target degrees must be synchronized, which means the ribbons either need to be degree-elevated or – if approximation is acceptable – degree-reduced.

If we want to ensure accurate boundary reproduction, we use a template with sufficient depth so that only degree elevations are necessary. The maximum of $(d_i^I - d_i^{T2})$ determines how many times the *T2* template need to be refined for this to be the case. We show a simple example on Figure 5 where the maximum difference between the input degrees (Figure 5a) and the T2 target degrees (Figure 5b) is 2; consequently a *T4* template (Figure 5c) will be sufficient to reproduce the input ribbons.

After we have matched the input and target degrees, the depth of the template is determined, together with the topology of the interior control structure. Our next task is to associate blend functions, as well as initial 3D positions to the control points.

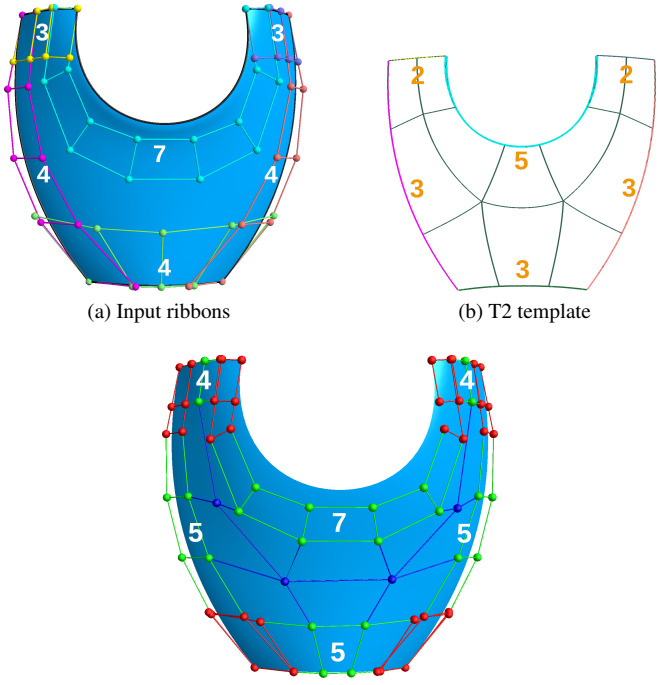


(a) Input ribbons (b) T2 template

(c) Final *T4* patch

Figure 5: Synchronizing the target and the input degrees.

## 5. Template blending functions

In this section we describe how to assign blending functions to interior control points (CPs) of the template-based structure. We first present a color-coded arrangement of CPs that helps explaining how blending functions are constructed. Note that the control structures of convex GB patches [3] and the proposed MAT-based GB patches are fairly similar. As shown in Figure 6, both are represented by a layer-based structure, the main difference being whether a single central CP or a set of skeleton CPs is given in the middle. (Another difference is the possibility of incompatible corners in CD-GB patches, although convex GB patches can also handle these thanks to the rational weights (Eq. 3) – see Hettinga and Kosinka [11].)

In our example there are four layers. The two outermost layers are determined by the input ribbons (as we deal here with $G^1$ boundaries). The first layer defines the boundary curves (green and red), the second the cross-derivative functions (cyan and red). The remaining CPs are called *interior* CPs, where we distinguish between the innermost *skeleton* CPs (blue) and the remaining, *intermediate* ones (yellow and orange), lying

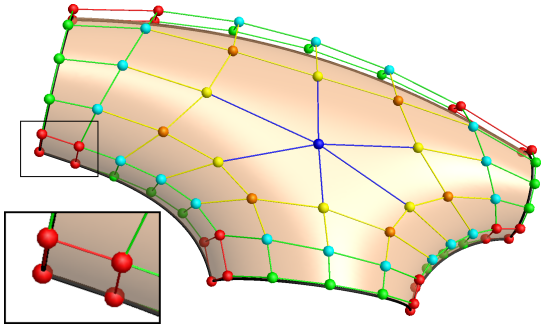

(a) Convex GB patch

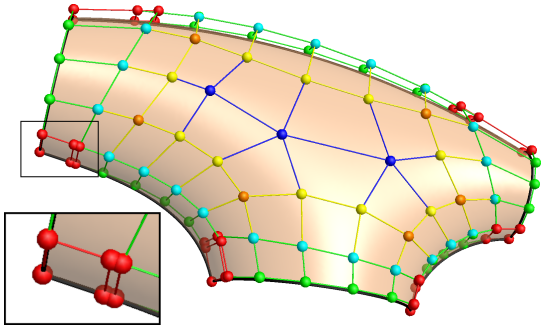

(b) Template-based CD-GB patch

Figure 6: Control point layer structures. Note that the CD-GB patch can have 'incompatible' corner derivatives, resulting in duplicated CPs (red).

between the ribbon CPs and the skeleton. The intermediate/interior control points $\mathbf{C}_l^{\text{Int}}$ can also be designated by $\mathbf{C}_{j,k}^{i}$, similarly the exterior CPs, where $i$ denotes the side the CP is associated with, $j \in \{0, \dots, d_i^T\}$ is the longitudinal index, and $k \in \{0, \dots, \lfloor D/2 \rfloor - 1\}$ is the layer index.

While some control points have only one associated $(i, j, k)$ triple (yellow in Fig. 6b), others have several: 'corner' CPs have two associated sides (orange in Fig. 6b), and skeleton CPs (blue in Fig. 6b) have three or more. Note that for a given CP the layer index $(k)$ is the same in all index triples. Let us denote the related index set with $V_l = \{(i, j, k) \,|\, \mathbf{C}_{j,k}^{i} = \mathbf{C}_l^{\text{Int}}\}$; this motivates the following definition for the blending functions in Eq. 6:

$$\omega_l(u, v) = \frac{1}{|V_l|} \sum_{(i,j,k) \in V_l} B_j(s_i) \cdot B_k(h_i). \tag{7}$$

In Figures 7–8 we demonstrate the concept of distributing weight deficiency by means of a test surface with three skeleton CPs (Fig. 8). Observe that the weight deficiency function determined by the ribbons is equal to the sum of the three interior blend functions, visualized as level surfaces over the domain (Fig. 7). The isocurves of the function assigned to the middle skeleton CP have also been mapped onto the surface in Fig. 8, illustrating the effect of the blending function on the surface shape.

## 6. Positioning template control points in 3D

While the representation itself allows arbitrary placement of the interior control points, it is useful to have an automated process to set them, based on solely the boundary constraints. Section 6.1 presents an approach similar to the one in the original GB paper [3]. We also describe some useful editing methods in Section 6.2 for simultaneous repositioning of the interior control points.

### 6.1. Initial setting by progressive depth elevation

In this section we describe a method for setting (initial) 3D positions for the control points of each template. While CPs in the outermost layers are essentially fixed by $G^1$ interpolation constraints, CPs in the interior are initially underdetermined. Taking inspiration from the degree elevation procedure of GB patches [3], we position them by progressive refinement of the interconnected control structure. Note that the proposed degree elevation procedure does *not* preserve the surface shape, and its purpose is to set the template CPs to an initial position.

As a first step, we initialize the template of depth 3 by degree elevating/reducing the input Bézier ribbons to the target longitudinal degrees $d_i^3$, and cross-degree $D = 3$ (in this section we use the simplified notation $d^D := d^{TD}$ for the target degrees).

We continue by elevating the depth, first from 3 to 4, then from 4 to 5 and so on. In what follows, we describe the general procedure for elevating the depth from $D$ to $D + 1$. The procedure is illustrated for the case of going from a template of even depth to a template of odd depth on Figure 9b, and for the case of going from odd to even on Figure 9c.

The two outermost layers of CPs (shown in red and green) are always set from the input ribbons by elevating them to target degrees $d_i^{D+1} = d_i^D + 1$ and cross-degree $D + 1$, so only interior control points $\mathbf{C}_l^{\text{Int},D+1}$ (shown in yellow and blue) are left to be determined. Recall that the usual degree elevation rule for Bézier surfaces defines a new CP within each quad face of the control structure – we generalize this approach from the tensor-product setting to general MAT-based structures.

A crucial observation is that similarly to the blends/control points of the previous section, each face of the depth $D$ template (or, equivalently, each vertex of the depth $D + 1$ template) can be associated with multiple boundaries with associated face indices $F_l = \{(i, j, k) \,|\, \mathbf{C}_{j,k}^{i,D+1} = \mathbf{C}_l^{\text{Int},D+1}\}$ and target degrees $d_i^D + 1$. For each associated face index, we define new vertices using the usual Bézier degree elevation rules raising the longitudinal degree to $d_i^D + 1$ and the cross-degree to $D + 1$:

$$\begin{aligned}\mathbf{C}_{j,k}^{i,D+1} = &\frac{j}{d_i^D + 1}\frac{k}{D+1}\mathbf{C}_{j-1,k-1}^{i,D} + \\ &\left(1 - \frac{j}{d_i^D + 1}\right)\frac{k}{D+1}\mathbf{C}_{j,k-1}^{i,D} + \\ &\frac{j}{d_i^D + 1}\left(1 - \frac{k}{D+1}\right)\mathbf{C}_{j-1,k}^{i,D} + \\ &\left(1 - \frac{j}{d_i^D + 1}\right)\left(1 - \frac{k}{D+1}\right)\mathbf{C}_{j,k}^{i,D}.\end{aligned} \tag{8}$$

Within 'corner' quads corresponding to two sides with indices $(i_1, j_1, k_1)$ and $(i_2, j_2, k_2)$ and target degrees $d_{i_1}^D \neq d_{i_2}^D$, degree elevation might result in two different control point positions, so a simple averaging is applied:

$$\mathbf{C}_l^{\text{Int},D+1} = \frac{1}{2}\left(\mathbf{C}_{j_1,k_1}^{i_1,D+1} + \mathbf{C}_{j_2,k_2}^{i_2,D+1}\right). \tag{9}$$

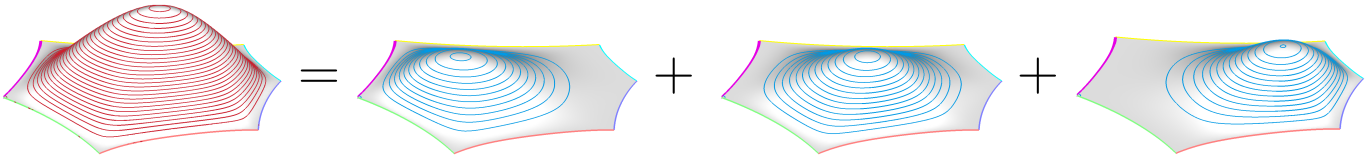

Figure 7: Illustration of distributing weight deficiency.

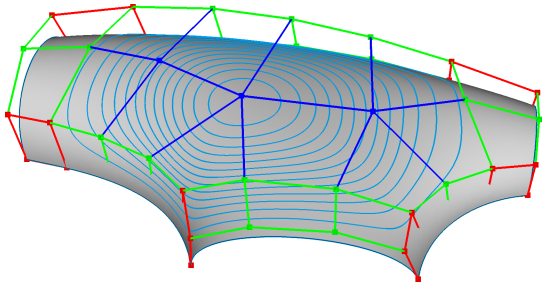

Figure 8: Interior blend function mapped onto a surface.

When elevating from odd to even, the innermost faces of the odd template (i.e., those associated with skeleton vertices) can have more than four sides, so simple Bézier elevation rules cannot be applied to them. One possibility – following the example of GB patches [3] – is to simply fix the position of these control points for all templates. This is however not recommended, because depth elevations might cause the intermediate CPs to eventually 'fold over' the fixed skeleton. Another alternative is taking the centroid $\hat{\mathbf{C}}_l$ of the polygon, but it leads to rapid flattening of the patch interior as depth is increased. We found that better results are achieved by averaging the polygon centroid with the corresponding CP from the previous (even) template:

$$\mathbf{C}_l^{\mathrm{Int},D+1} = \frac{1}{2}\left(\mathbf{C}_l^{\mathrm{Int},D-1} + \hat{\mathbf{C}}_l\right), \tag{10}$$

which is the scheme used to generate the examples shown in the paper.

### 6.2. Editing

In our experience, even with the proposed initial CP distribution, the surface interior can become flat as refinement progresses, which we attribute to the relatively low value of the interior blend functions. While direct optimization of surface fairness would be challenging due to the non-explicit local parameters, it is also the case that the shape can often be improved by careful manual positioning of the interior control points. We discuss three different approaches to manual editing.

First, the control points could be edited *individually*. For complex templates, however, the number of interior CPs can grow rapidly with depth and individual editing eventually becomes impractical.

Another possibility is *hierarchical editing*, i.e., modifying the CPs of a coarser template and thus editing entire groups of CPs at the same time through refinement, similarly to subdivision surfaces [36]. An example of hierarchical editing is shown in Figure 10.

In our experience working with different refinement levels can be difficult, and it is preferable to simultaneously move groups of control points within a single level of hierarchy. As already mentioned, for GB patches it was possible to use the same 'central' CP for all depths and use it to edit the entire control structure for any given depth, but this is no longer possible for more general templates. To reproduce the desired behavior, we implemented a design interface similar to the *proportional editing* found in Blender [37].

The idea is to propagate the displacement of each CP to its neighbors, gradually decreasing the displacement magnitude depending on the discrete distance from the displaced CP. The decrease of the magnitude is controlled by a displacement *falloff function*, which we choose to determine by minimizing a discrete harmonic energy over the control mesh (but alternative fallout functions could also be employed, depending on the designer's preferences). More formally, when a selected CP is displaced by a vector $\mathbf{d}$, the displacements over the rest of the template are defined as $\mathbf{C}_i^{\mathrm{after}} = \mathbf{C}_i^{\mathrm{before}} + f_i\mathbf{d}$, where the falloff factors $f_i$ satisfy a discrete Laplace equation

$$\mathbf{L}\mathbf{f} = 0 \tag{11}$$

under the constraint that the factor of the selected CP is fixed to the value 1, while those outside of a (user-defined) range of influence around the selected CP are fixed to 0. For the matrix $\mathbf{L}$ we choose a uniform (graph) Laplacian, following Worchel and Alexa [38, Ch. 3.3]. The falloff functions can simply be precomputed and cached when the template is initialized. An example of proportional editing for a template of depth 6 is shown on Figure 11.

## 7. Discussion

In this Section we show further examples of editing and discuss some possible variations of the proposed concept.

### 7.1. Weight deficiency

Weight deficiency (WD) is defined over the curved domain. It is a peculiar function that characterizes to what extent the patch interior is determined by the ribbons. At places where WD is 'small', the ribbons are 'strong' and consequently the interior CPs can modify the patch interior only to a 'small' extent. At other places, where WD is 'large', the ribbons are 'weak' and they underdetermine the shape, thus a large WD can be distributed and the interior CPs will strongly affect the patch. Note that by varying the local parameterization of the domain it is possible to change the WD function, and indirectly the strength of the interior CPs.

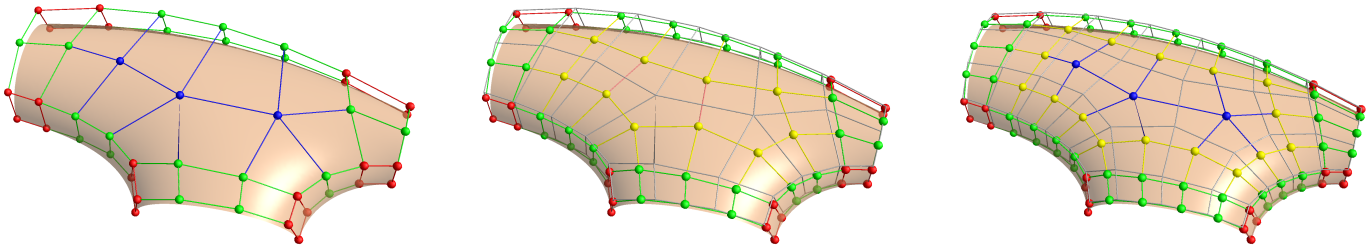

(a) Depth-4 template (b) Even → odd (4 → 5) (c) Odd → even (5 → 6)

Figure 9: Illustration of template depth elevation. Gray colors indicate the previous template.

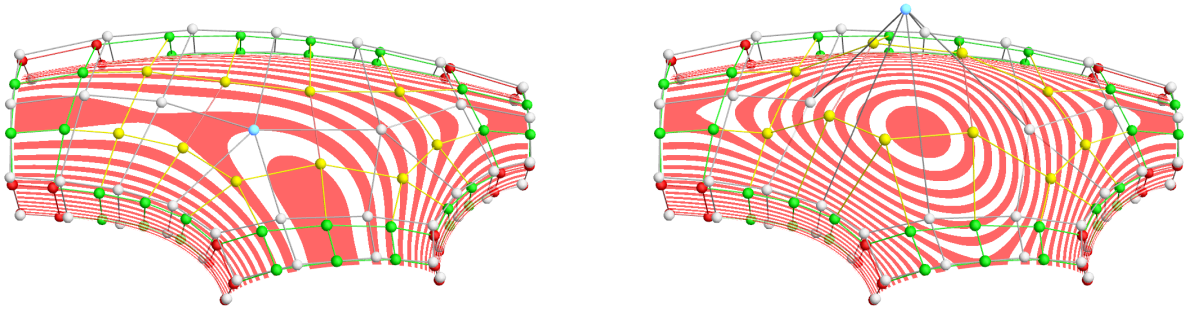

(a) Before editing (b) After editing

Figure 10: Example of hierarchical editing via a previous template (in grey) – surrounding yellow CPs are lifted. Surface slicing is shown.

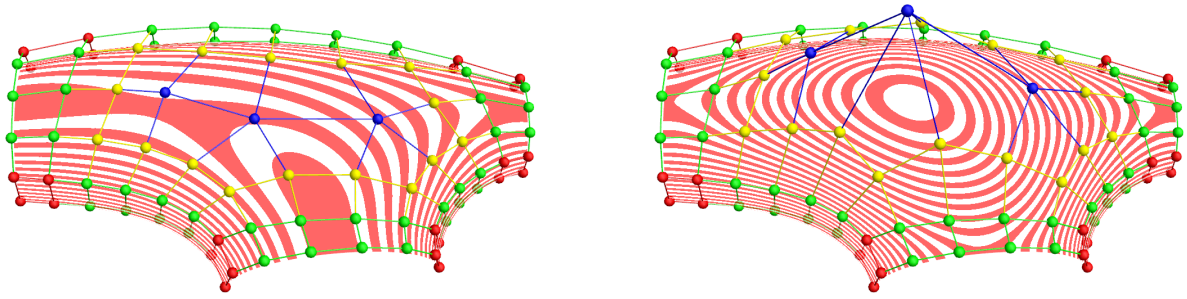

(a) Before editing (b) After editing

Figure 11: Example of proportional editing of a template – surrounding blue and yellow CPs are dragged along. Surface slicing is shown.

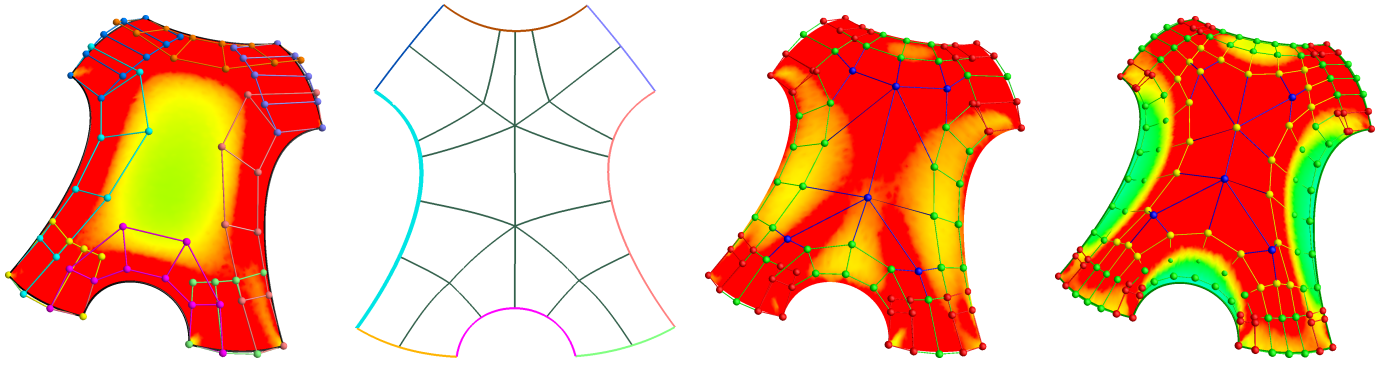

(a) CD-GB patch (b) Curved domain (c) With interior controls (d) Depth elevation and modification

Figure 12: Setback vertex blend example. Colors indicate mean curvature.

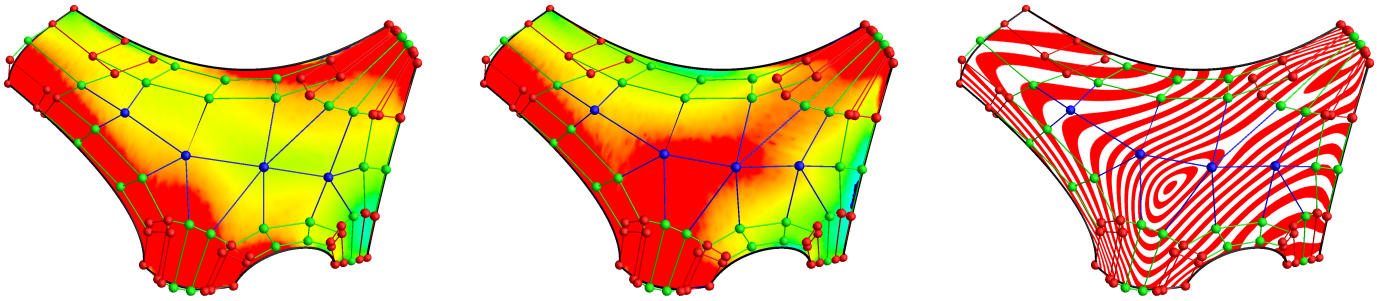

(a) Initial model (b) After modification (skeleton CPs lifted) (c) Isophote lines

Figure 13: Car body panel example.

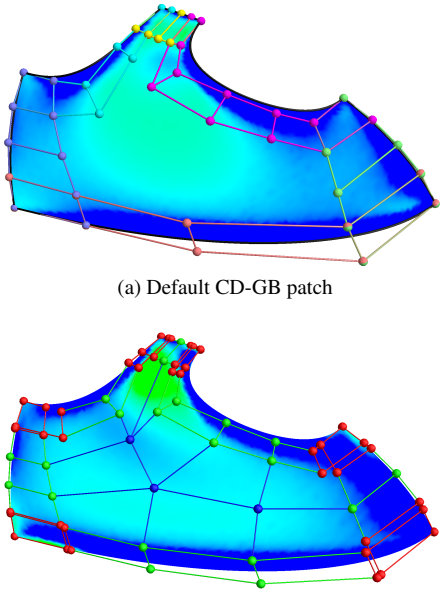

(a) Default CD-GB patch

(b) Default MAT-GB patch

Figure 14: Comparison of default patches. Colors indicate mean curvature.

### 7.2. Editing examples

A setback vertex blend model with a branching skeleton structure is shown in Figure 12. The original CD-GB patch has a flat 'plateau' in the interior, indicated by the green region of the mean curvature map (Fig. 12a). The quartic template (Fig. 12b) adds several interior control points, creating a nice curvature to the middle of the patch (Fig. 12c). With a refinement to a sextic template and manual modification of the interior, new shape features can also be introduced (Fig. 12d).

A similar situation arises for the car body panel model (Fig. 13; the corresponding domain is shown in Fig. 3): the right side is initially somewhat flat (Fig. 13a), but after slight modification of the interior (blue) control points, the mean curvature distribution (Fig. 13b) and the isophote distribution (Fig. 13c) can both be improved.

To compare the 'default' surfaces generated by the original CD-GB scheme and the proposed MAT-based representation we show a panel of an iron model on Figure 14.

### 7.3. MAT editing operations

Our approach automatically generates a control net topology, but the user may not be satisfied with its resolution, and might prefer to add further degrees of freedom, or conversely, may prefer to simplify the structure. We have implemented the following topological operations:

- *Simplify*. Deletes a central edge from the MAT.
- *Refine*. Splits a corner or a central edge.

Figure 15 shows a sequence of these two operations, where first a very short edge is removed (thereby removing redundant controls) and then a long edge is refined (adding further degrees of freedom). These operations can be applied either manually (as was done to produce some of the examples in the paper), or as part of an automatic procedure.

### 7.4. Low-degree approximative variant

Depending on the application, it may not be essential to exactly interpolate the original Bézier boundaries and cross-derivatives. When for the template of a given depth $d_i^T < d_i^I$ holds, the original boundary constraints can be approximated using $d_i^T + 1$ control points in the longitudinal direction. Note that lower polynomial degrees are generally favorable as surface quality is better controlled and the patch is easier to modify.

### 7.5. Mixed-degree variant

Twist-compatible cross-derivative constraints at corners between boundaries of different degrees result in duplicated control points, as in Figure 12c above. Such duplication can be avoided by using *mixed-degree* blending functions combining the degrees of the adjacent sides:

$$\hat{\gamma}_{ijk}(u,v) = \mu_j^i(u,v)\cdot B_j^{d_i}(s_i)\left((1-\alpha_j)B_k^{d_{i-1}}(h_i)+\alpha_j B_k^{d_{i+1}}(h_i)\right), \quad (12)$$

where $\alpha_j$ ($j = 0,\ldots,d_i$) are (constant) weights satisfying

$$\begin{aligned} \alpha_j &= 0, & j &< 2, \\ \alpha_j &= 1, & j &> d_i - 2, \end{aligned} \quad (13)$$

with intervening values determined (e.g.) by linear interpolation. When using these mixed-degree blends, the control points in the second row need to be appropriately re-positioned to retain cross-derivative interpolation.

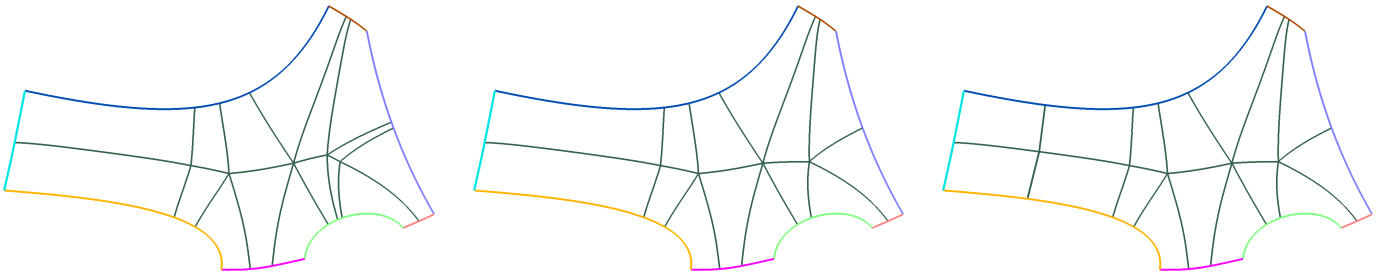

(a) Original MAT tiles (b) MAT simplification (edge removal) (c) MAT refinement (edge splitting)

Figure 15: Examples of MAT editing operations.

## Conclusion and future work

We have extended the Curved Domain Generalized Bézier (CD-GB) representation with additional interior controls, whose topological structure is automatically determined based on the boundary configuration. We described a scheme for distributing the weight deficiency generated by ribbon interpolants. We have also proposed algorithms for the initial positioning of the new control points, as well as their modification. The additional degrees of freedom are often indispensable for achieving good shape quality or adding interior detail, especially in cases where the number of sides is fairly large and/or interior control with a single central control point is simply not sufficient.

The method as described satisfies $G^1$ boundary constraints; generalizing it to higher-order continuity should be straightforward (although we note that for many practical applications approximate $G^2$ continuity is often considered sufficient, sometimes even preferable over exact curvature continuity, see e.g. [39]). Support for 'smooth' corners (where two adjacent boundaries share the same tangent) would be another important step, as highly curved boundaries are hard to model with single polynomial segments, and this would also lead naturally to a generalization to B-spline boundaries. We believe that the parametric MAT that we introduce could be useful for a variety of practical applications; for example, as an alternative approach for the initial setting of cross-derivatives in [39]. Finally, the proposed scheme for distributing a weight function among control points is fairly general and could also be applied to other (e.g. transfinite) multi-sided surfaces as well.

## Acknowledgments

This project has been supported by the Hungarian Scientific Research Fund (OTKA, No. 145970). The authors would like to acknowledge the significant programming contribution of György Karikó for extending our prototype surfacing system Sketches (ShapEx Ltd., Budapest).

## References

[1] Várady, T, Salvi, P, Vaitkus, M. Genuine multi-sided parametric surface patches – a survey. Computer Aided Geometric Design 2024;110:102286. doi:10.1016/j.cagd.2024.102286.

[2] Zheng, J, Ball, AA. Control point surfaces over non-four-sided areas. Computer Aided Geometric Design 1997;14(9):807–821. doi:10.1016/S0167-8396(97)00007-1.

[3] Várady, T, Salvi, P, Karikó, G. A multi-sided Bézier patch with a simple control structure. Computer Graphics Forum 2016;35(2):307–317. doi:10.1111/cgf.12833.

[4] Várady, T, Salvi, P, Vaitkus, M, Sipos, Á. Multi-sided Bézier surfaces over curved, multi-connected domains. Computer Aided Geometric Design 2020;78:101828. doi:10.1016/j.cagd.2020.101828.

[5] Vaitkus, M, Várady, T, Salvi, P, Sipos, Á. Multi-sided B-spline surfaces over curved, multi-connected domains. Computer Aided Geometric Design 2021;89:102019. doi:10.1016/j.cagd.2021.102019.

[6] Goldman, R. Multisided arrays of control points for multisided Bézier patches. Computer Aided Geometric Design 2004;21(3):243–261. doi:10.1016/j.cagd.2003.10.003.

[7] Loop, CT, DeRose, TD. A multisided generalization of Bézier surfaces. ACM Transactions on Graphics (TOG) 1989;8(3):204–234. doi:10.1145/77055.77059.

[8] Krasauskas, R. Toric surface patches. Advances in Computational Mathematics 2002;17:89–113. doi:10.1023/A:1015289823859.

[9] Karčiauskas, K. Rational *M*-patches and tensor-border patches. In: Topics in Algebraic Geometry and Geometric Modeling; vol. 334 of *Contemporary Mathematics*. AMS; 2003, p. 101–130. doi:10.1090/conm/334.

[10] Sabin, MA. Non-rectangular surface patches suitable for inclusion in a B-spline surface. In: Eurographics Conference Proceedings. Eurographics Association; 1983,doi:10.2312/eg.19831004.

[11] Hettinga, GJ, Kosinka, J. Multisided generalisations of Gregory patches. Computer Aided Geometric Design 2018;62:166–180. doi:10.1016/j.cagd.2018.03.005.

[12] Qin, K, Li, Y, Deng, C. Blending Bézier patch for multi-sided surface modeling. Computer Aided Geometric Design 2023;105:102222. doi:10.1016/j.cagd.2023.102222.

[13] Salvi, P, Várady, T. Multi-sided Bézier surfaces over concave polygonal domains. Computers & Graphics 2018;74:56–65. doi:10.1016/j.cag.2018.05.006.

[14] Huerta, A, Belytschko, T, Fernández-Méndez, S, Rabczuk, T, Zhuang, X, Arroyo, M. Meshfree methods. In: Encyclopedia of Computational Mechanics Second Edition. Wiley; 2018, p. 1–38. doi:10.1002/9781119176817.ecm2005.

[15] Jacobson, A, Baran, I, Popovic, J, Sorkine, O. Bounded biharmonic weights for real-time deformation. ACM Transactions on Graphics (TOG) 2011;30(4):78. doi:10.1145/2010324.1964973.

[16] Salvi, P. Editing the interior of arbitrary surfaces using $C^\infty$ displacement blends. In: Proceedings of the Workshop on the Advances of Information Technology. BME; 2021, p. 35–38.

[17] Várady, T, Salvi, P, Kovács, I. Enhancement of a multi-sided Bézier surface representation. Computer Aided Geometric Design 2017;55:69–83. doi:10.1016/j.cagd.2017.05.002.

[18] Salvi, P, Várady, T. Multi-sided surfaces with fullness control. In: Proceedings of the Eighth Hungarian Conference on Computer Graphics and Geometry. NJSZT; 2016, p. 61–69.

[19] Ball, AA, Zheng, J. Degree elevation for *n*-sided surfaces. Computer Aided Geometric Design 2001;18(2):135–147. doi:10.1016/S0167-8396(01)00020-6.

[20] Salvi, P. Intuitive interior control for multi-sided patches with arbitrary

boundaries. Computer-Aided Design and Applications 2024;21(1):143–154. doi:10.14733/cadaps.2024.143-154.

[21] Várady, T, Salvi, P, Rockwood, A. Transfinite surface interpolation with interior control. Graphical Models 2012;74(6):311–320. doi:10.1016/j.gmod.2012.03.003.

[22] Martin, F, Reif, U. Trimmed spline surfaces with accurate boundary control. In: Geometric Challenges in Isogeometric Analysis; vol. 49 of *Springer INdAM Series*. 2022, p. 123–148. doi:10.1007/978-3-030-92313-6_6.

[23] Höllig, K, Reif, U, Wipper, J. Weighted extended B-spline approximation of Dirichlet problems. SIAM Journal on Numerical Analysis 2001;39(2):442–462. doi:10.1137/S0036142900373208.

[24] Campen, M. Partitioning surfaces into quadrilateral patches: A survey. Computer Graphics Forum 2017;36(8):567–588. doi:10.1111/cgf.13153.

[25] Lyon, M, Campen, M, Kobbelt, L. Quad layouts via constrained T-mesh quantization. Computer Graphics Forum 2021;40(2):305–314. doi:10.1111/cgf.142634.

[26] Zhang, C, Chai, S, Liu, L, Fu, XM. Quad meshing with coarse layouts for planar domains. Computer-Aided Design 2021;140:103084. doi:10.1016/j.cad.2021.103084.

[27] Shen, J, Kosinka, J, Sabin, MA, Dodgson, NA. Conversion of trimmed NURBS surfaces to Catmull–Clark subdivision surfaces. Computer Aided Geometric Design 2014;31(7-8):486–498. doi:10.1016/j.cagd.2014.06.004.

[28] Buchegger, F, Jüttler, B. Planar multi-patch domain parameterization via patch adjacency graphs. Computer-Aided Design 2017;82:2–12. doi:10.1016/j.cad.2016.05.019.

[29] Tarini, M. Closed-form quadrangulation of $n$-sided patches. Computers & Graphics 2022;107:60–65. doi:10.1016/j.cag.2022.06.015.

[30] Tam, T, Armstrong, CG. 2D finite element mesh generation by medial axis subdivision. Advances in engineering software and workstations 1991;13(5-6):313–324. doi:10.1016/0961-3552(91)90035-3.

[31] Rigby, D. Topmaker: A technique for automatic multi-block topology generation using the medial axis. In: Fluids Engineering Division Summer Meeting; vol. 36967. 2003, p. 1991–1997. doi:10.1115/FEDSM2003-45527.

[32] Quadros, W, Ramaswami, K, Prinz, F, Gurumoorthy, B. LayTracks: a new approach to automated geometry adaptive quadrilateral mesh generation using medial axis transform. International journal for numerical methods in engineering 2004;61(2):209–237. doi:10.1002/nme.1063.

[33] Fogg, HJ, Armstrong, CG, Robinson, TT. Enhanced medial-axis-based block-structured meshing in 2-D. Computer-Aided Design 2016;72:87–101. doi:10.1016/j.cad.2015.07.001.

[34] Gregory, JA. Smooth interpolation without twist constraints. In: Computer Aided Geometric Design. University of Utah; 1974, p. 71–87. doi:10.1016/B978-0-12-079050-0.50009-6.

[35] Siddiqi, K, Pizer, S. Medial Representations: Mathematics, Algorithms and Applications; vol. 37 of *Computational Imaging*. Springer; 2008. doi:10.1007/978-1-4020-8658-8.

[36] Zorin, D. Modeling with multiresolution subdivision surfaces. In: ACM SIGGRAPH 2006 Courses. 2006, p. 30–50. doi:10.1145/1185657.1185673.

[37] Blender Online Community, . Blender 4.0 Reference Manual. 2024. URL: https://docs.blender.org/manual/; Section Editors / 3D Viewport / Controls / Proportional Editing.

[38] Worchel, M, Alexa, M. Differentiable rendering of parametric geometry. ACM Transactions on Graphics (TOG) 2023;42(6):1–18. doi:10.1145/3618387.

[39] Salvi, P, Vaitkus, M, Várady, T. Constrained modeling of multi-sided patches. Computers & Graphics 2023;114:86–95. doi:10.1016/j.cag.2023.05.020.